Association of Interannual and Interdecadal Variations of Global-Mean Temperature with Tropical Pacific SST Appearing in a Model and Observations

IN-SIK KANG

Department of Atmospheric Sciences, Seoul National University, Seoul, Korea

(Manuscript received 14 October 1994, in final form 15 August 1995)

ABSTRACT

Long-term variations of global-mean air temperature at the surface are investigated using data from a GFDL coupled ocean–atmosphere model 139-year simulation and the observed datasets of surface air temperature over the globe for 139 years and tropical Pacific SST for 42 years. The global-mean surface air temperatures of both the model and observation are characterized by interdecadal oscillations with timescales of about 20 years and 10 years and interannual fluctuations with timescales of 3–6 years. The global-mean temperature anomaly (GMTA) is related to the first empirical orthogonal function mode of surface air temperature over the globe, which, in turn, is associated with the first eigenmode of SST over the tropical Pacific. The first eigenmode of tropical Pacific SST has a spatial pattern similar to that during a mature phase of El Niño, and its associated time series is characterized by the 3–6-yr interannual and interdecadal timescales. It is demonstrated that both interannual and interdecadal variations of the GMTA are associated with the corresponding variations of tropical Pacific SST. Comparisons of the model results with observed counterparts show that the coupled model has a capability of simulating many important features of surface air temperature variations over the globe and SST fluctuations over the tropical Pacific, except that the interannual variations of the model with timescales of 3–6 years are relatively weak.

The sampling error of the observed GMTA for the 139 years 1854–1992 due to inhomogenous spatial distribution of the data over the globe is examined by using the coupled model data. Although the sampling error of monthly mean GMTA is not small even for recent years, the long-term variations of GMTA with timescales longer than few years are not much affected by the sampling problem.

1. Introduction

Recently, the research interest in global climate variability has been extending from interannual to interdecadal timescales. The interannual variability in connection with the ENSO has been extensively studied for past several decades. On the other hand, the interdecadal variation has been documented more recently by several authors (Folland et al. 1984; Newell et al. 1989; Ghil and Vautard 1991; Keppenne and Ghil 1991; and others). In particular, Ghil and Vautard (1991) showed that the time series of global mean air temperature for past 135 years has a distinctive interdecadal oscillation with a timescale of about 20 years, as well as 5–6 year interannual variation. Recent interest of the interdecadal oscillation may arise from the problem in separating the global warming trend and natural variability in observed long-term time series. The present study is aimed at identifying the interdecadal and interannual oscillations of global mean surface air temperature in a coupled ocean–atmosphere model and comparing them with observed temperature oscillations.

The association of the interdecadal and interannual variations of global mean temperature with those of Pacific sea surface temperature (SST) is also investigated in the present study. Since Bjerknes (1966), the association of the interannual atmospheric variability over the globe with the fluctuations of the tropical Pacific has been demonstrated by many authors (e.g., Horel and Wallace 1981; Namias et al. 1988). More recently, several studies indicate that the Pacific ocean also fluctuates with interdecadal timescales. Keppenne and Ghil (1991) found a regular oscillation of interdecadal envelope that modulates the amplitudes of the annual and semiannual cycle of the ENSO index. They related the interdecadal oscillation of the ENSO index to the 17-yr oscillation of global mean temperature found by Ghil and Vautard (1991). Nitta and Yamada (1989) showed that the SST anomalies over the tropical Pacific in the 1980s are warmer than those in the 1960s and early 1970s and demonstrated that the tropical and extratropical atmospheric indices associated with the El Niño before and after the mid-1970s are different from each other. More recently, Jacobs et al. (1994) showed the existence of trans-Pacific propagation of planetary-scale oceanic waves with a time-

Corresponding author address: Prof. In-Sik Kang, Department of Atmospheric Sciences, Seoul National University, Kwanak-ku, 151 Seoul, Korea.

scale of a decade. They further demonstrated that a major El Niño event such as occurred during 1982–1983 has extratropical and decadal components. Those studies mentioned above indicate the major role of tropical Pacific SST in the interdecadal as well as interannual fluctuations of atmospheric and oceanic indices over the globe.

When investigating the variation of observed global mean temperature anomaly (GMTA), a sampling problem is often encountered due to incomplete spatial coverage of the data over the globe. In fact, there are many missing data points in observation, particularly over the oceans, and also the spatial coverage of the observed data has changed in time. Madden and Meehl (1993) examined the sampling error of the global mean, particularly in determining global warming signal. They concluded that the inhomogenous spatial sampling produces less than 2% bias of global warming for the recent years after 1950. During this period, the data coverage changed little, but the sampling problem can be more serious for the data period of nineteenth century. Elsner and Tsonis (1991), in fact, questioned the quality of global mean temperature data before 1880. To consider the data problem for late nineteenth century, Hansen and Lebedeff (1987) examined the effect of poor spatial sampling on global mean temperature using output from a 100-yr GCM run. For yearly averages, they found the root-mean-square (rms) error of 0.07°C for station locations during the 1880s and 0.02°C for those during the 1960s. On the other hand, a similar examination by Madden et al. (1993) showed that the rms errors are 0.224°C in the 1860s and 0.045°C after 1950. The large differences between the two studies seem to be related to the use of different time means and different model data. The present study made another estimate of the sampling error using a similar method to those of the above two studies but using a more realistic model, an ocean–atmosphere-coupled GCM, for the study of decadal variability. The results will be compared with those of previous studies, and the estimated error of observed global-mean temperature (GMT) due to the poor spatial coverage of observed data will be discussed before examining the observed GMT.

Section 2 introduces the model and the observed data utilized in the present study. The coupled atmosphere–ocean model used in the present study and the model experiment are briefly described in this section. In section 3, the fluctuations of global-mean surface air temperature that appeared in the model are examined by using a power spectrum analysis and the results are compared with those of observation. The sampling error of the observed global mean temperature is also examined. Section 4 examines the spatial pattern of surface air temperature anomaly associated with the global mean fluctuations. In section 5, the fluctuations of surface air temperature over the globe are related to the principal mode of tropical Pacific SST fluctuations. Section 6 provides the summary of the present study and concluding remarks.

2. Model and data

The dataset utilized in the present study was obtained from a long-term simulation of a GFDL ocean–atmosphere coupled model. The atmosphere model is a spectral model with a rhomboidal truncation of wavenumber 15 and nine levels in the vertical. It includes a comprehensive set of physical processes such as radiation, convection, and surface processes. The insolation imposed at the top of the atmosphere has seasonal variation but no diurnal variation. Details of the model structure can be found in Manabe et al. (1990). The ocean model is a gridpoint model with a resolution of 4.5° in latitude and 3.75° in longitude and 12 vertical levels. The basic structure of the ocean model is similar to that of Bryan and Lewis (1979). Sea ice is treated with a prognostic system similar to Bryan (1969).

In coupling the two models, the surface fluxes of heat and water at the ocean surface are adjusted to ensure a realistic simulation of observed SST over the globe. The adjustment varies geographically and with season but does not change interannually. With the coupled model, long-term simulations have been carried out at GFDL with different states of atmospheric CO_2 (Manabe et al. 1991). In the present study, we used the data taken from the model experiment carried out with a normal CO_2 concentration fixed for the entire simulation period. This experiment is the one referred to as the "standard run" in Manabe et al.

The data taken from the model historical record of data are the monthly means of surface air temperature and sea surface temperature over the globe for 139 years. The reason for using 139-yr data is to make the data period the same as the period of available observation. A long historical record of surface air temperature over the globe for the period from January 1854 to December 1992 was obtained from Carbon Data Center of the Oak Ridge National Laboratory. The spatial resolution of the observed data is 5° in longitude and 5° in latitude. Details of the observed data, particularly over the land, can be found in Jones et al. (1986). The observed SST data utilized in the present study is the one reconstructed recently at National Center for Environmental Prediction (NCEP). It was obtained by applying a new interpolation method, based on spatial patterns from empirical orthogonal functions of SST anomalies for the period of 1982–1992, to the monthly SST of Comprehensive Ocean–Atmospheric Data Sets (COADS) for the period of 1950–1992. The reconstructed fields have lower rms differences than the SST derived from the traditional NCEP analysis of optimum interpolation (T. Smith, personal communication). The annual mean SST for 1950–1992 over the tropical Pacific are obtained from the monthly SST and utilized in the present study.

3. Fluctuations of global-mean surface air temperature

In this section, the characteristics of global-mean temperature fluctuations simulated by the coupled model are examined and compared with those of observation. Figure 1 shows the time series of global-mean temperature anomaly (GMTA) for 139 years. The time series at the top (Fig. 1a) of the figure is the model GMTA, and the time series at the bottom (Fig. 1c) is the GMTA obtained with observed data. The model anomaly is defined as the departure from the 139-yr mean, and the observed anomaly is the departure from the mean of 1951–1970 reference period. The observed data has missing data points, therefore the global mean ($\bar{T}$) is obtained by the area mean of the data available over the globe, $\bar{T} = (\Sigma_i T_i \cos\theta_i)/(\Sigma_i \cos\theta_i)$, where i is the grid point of the data available at each month. Figure 2 shows the month to month variation of the total number of observed data points. The spatial resolution of the observed data is 5° in longitude and 5° in latitude and the total number of data points over the globe is 2592. The number of data points has increased almost linearly with time for 100-yr period from mid-nineteenth century to mid-twentieth century, and it has been almost constant for last 40 years. Also note that the number of data points decreased in recent years. The imperfect spatial coverage of the data can produce an error in the global mean. In particular, the interannual variability of GMTA can be biased by the variation of available data points in time. For example, relatively large month to month variability in the nineteenth century shown in the bottom of Fig. 1 can result from the small number of available data for that period (less than one-fifth of the total data points in the globe). An examination of such sampling error in the observed GMTA follows.

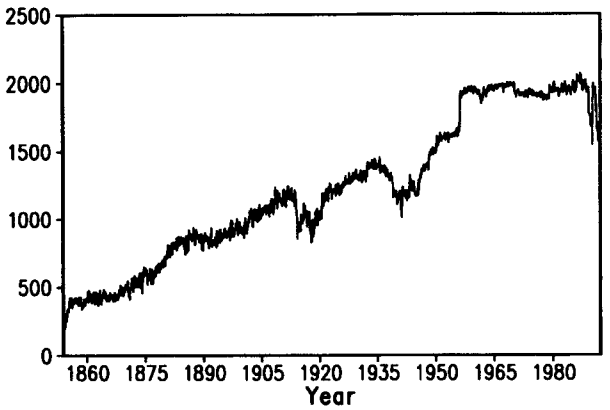

FIG. 2. Time series of the number of available observed data points over the globe.

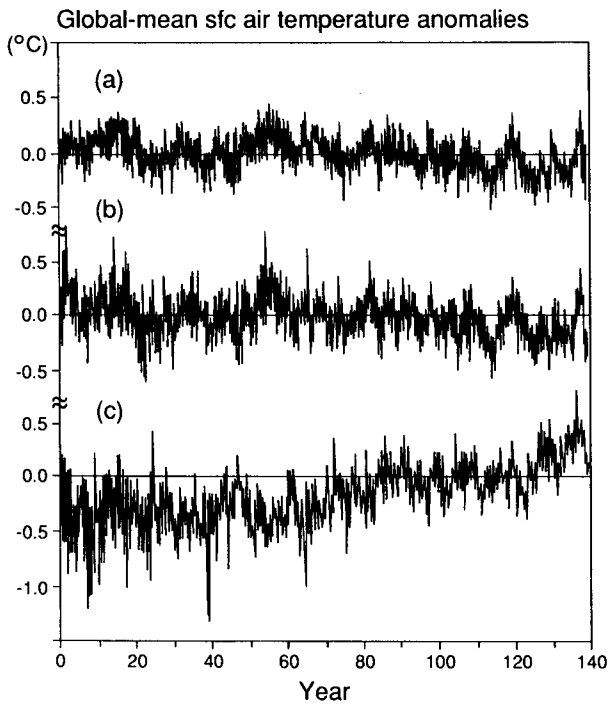

FIG. 1. (a) Time series of the monthly mean, globally averaged surface air temperature anomaly calculated from the model data. (b) As in (a) except for the global mean of the model averaged only over available observation data points each month from January 1854 to December 1992. (c) As in (b) except calculated with observed data.

The time series in Fig. 1b shows the GMTA of the model obtained by the area average of the data over the observed grid points for each month from January 1854 to December 1992. Here the first month of the model data corresponds to January 1854. In other words, we first masked out model data at the grid point where observed data were not available at each month, and then the global mean was calculated based on the modified model data. For this purpose, the model data was converted to the observed grid system by a linear interpolation method. Hereafter, the GMTA thus obtained is referred to as the sampled global mean. There are certain differences between the global total mean (Fig. 1a) and the sampled global mean (Fig. 1b), in particular, for early part of the time series. This indicates that the early part of the observed global-mean time series can be biased by insufficient samples. On the other hand, for the second half of the time series, when the number of data points is larger than one-half of the total number of grid points over the globe, two time series (a) and (b) are fairly similar to each other.

Although there are some differences between the monthly mean values of Figs. 1a and 1b, particularly for the early period, longer timescale variations of the GMTA appear to be similar to each other. To more clearly see the longer timescale variations, the annual-mean GMTA was computed for the time series of Figs. 1a and 1b and values are shown in Fig. 3. There are some differences in the magnitudes of (a) and (b) in

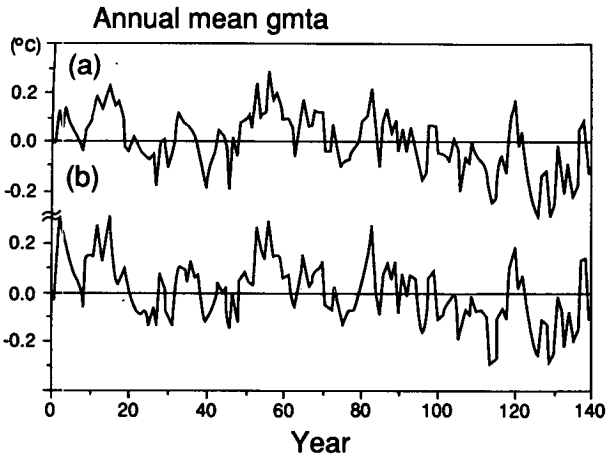

FIG. 3. (a) Time series of the annual mean, globally averaged surface air temperature anomaly of the model. (b) As in (a) except for the global mean averaged only over the observed data points.

Fig. 3, but year to year variation of the global total mean is well represented by the global mean obtained from the sampled data. The sampling error is examined in more detail with Table 1, which shows the time-mean error and rms error of the sampled global mean for each 20-yr segment. The rms errors in the table are estimated based on the annual means. As expected, the largest error appears in the first 20-yr period with the mean error of 0.031°C and the rms error of 0.082°C. After the first 20-yr period, the mean error is relatively small except for year 61–80, which corresponds to the period of 1914–1933 in actual observation. For recent 59 years after year 80, the value of absolute mean error plus two times the rms error does not exceed 0.07°C, indicating that the error of the annual-mean sampled GMTA seldom (probability less than 2.5%) exceeds 0.07°C for this period.

It will be interesting to compare the above results with those of Madden et al. (1993), who estimated the sampling error in a similar manner to the present study. Their rms errors, 0.224°C in the 1860s and 0.045°C after 1950, are much larger than the corresponding values in Table 1. But note that their rms errors are based on the *monthly* means for a 10-yr segment. In fact, the estimated rms errors of monthly means for 10-yr segments using the present data are 0.20°C for 1860s and 0.048°–0.055°C after 1950. These values are close to those of Madden et al., indicating that the differences between the values in Table 1 of the present study and Fig. 3 of Madden et al. result mainly from the use of different time means. For yearly averages, Hansen and Lebedeff (1987) obtained the rms errors of 0.07°C for the 1880s and 0.02°C for the 1960s, while corresponding values obtained from the present data are 0.05°C and 0.03°C, respectively. These differences are certainly due to the use of different model outputs.

It is also noted that Madden and Meehl (1993) estimated the sampling error of global warming trend for the 1950–1979 period. They showed that the sampling error does not exceed 2% of the global mean warming trend. However, the present study indicates that the sampling error of natural variability is relatively large. For the 1950–1979 period, the rms of annual-mean error (0.028°C) is 17% of the rms of annual-mean GMTA (0.164°C). Such a difference can be explained as follows. The spatial pattern of the warming trend is more or less fixed in time and large warming signals appear over the continents where relatively large numbers of samples are available. On the other hand, the spatial pattern of natural variability varies interannually, and the oceanic anomalies contribute a large portion of global mean anomaly. From the above results, it can be suggested that the sampling error in making global mean anomaly is not small even for recent years. However, it is noted that long-term variation of the global total mean (Fig. 3a) is well represented by the global mean obtained with the sampled data (Fig. 3b). The correlation coefficient between the two time series for the entire period is 0.93. It is also noted that the rms error of the sampled monthly mean GMTA is two to three times bigger than that of the annual-mean (not shown). With this reason, hereafter, we will utilize the annual-mean data for further analysis of the model and observed GMTA variability.

The characteristic timescales of the global-mean temperature variability are examined by using a power spectrum method. The power spectra of the model and the observed GMTA for the 139-yr period are shown in Figs. 4a and 4b, respectively. The model GMTA has spectral peaks at the periods of about 18, 10, and 3–6 years. In the figure, the lower line indicates the level of red noise, and the upper dashed line indicates the level that the estimated spectral density must exceed to reject a null hypothesis of red noise with 90% a priori confidence. In the figure, the 10- and 18-yr spectral peaks are at the 90% confidence level, and significant spectral peaks appear for certain spectral bands in the interannual timescales of 3–6 years. The spectral peaks of interannual and interdecadal timescales appear also in the observed GMTA, although there are certain differences between the two. In particular, the 18-yr oscillation of the model is shifted to the 22-yr period in the observation data, but the observed 22-yr spectral peak is not very significant. Interestingly, the 10-yr spectral peak appears both in the observation and the model data, and the spectral peak is pronounced particularly in the observation data. It is also noted that the observed GMTA has larger power in the interannual time bands of 2–7 years than the corresponding variability of the model. The small interannual variability of the model is due to the relatively small amplitude of ENSO-like oscillation appearing in the model (Lau et al. 1992). Overall, the statistically significant oscillations of observed GMTA appear at the timescales of 3–6 years

TABLE 1. The time-mean error and rms error of the sampled annual mean GMTA for each 20-yr segment (°C).

	Segment (yr)						
	1–20	21–40	41–60	61–80	81–100	101–120	121–139
Mean error	0.031	−0.005	−0.014	−0.038	−0.001	−0.013	0.015
rms error	0.082	0.052	0.038	0.043	0.033	0.029	0.026

and at about 10 years, and those timescales oscillations also appear in the coupled model.

It is noted that the power spectrum analysis of observed GMTA shows a spectral peak at the period of 22 years, but it is just above the red noise. However, Ghil and Vautard (1991) showed using the singular spectrum analysis (SSA) that the 20-yr oscillation is a leading eigenmode of the observed GMTA after the trend. It may be possible that the 20-yr oscillation is separated by SSA but not clearly by the power spectrum analysis because the amplitude of the 20-yr oscillation varies in time. Note that the principal time series obtained with SSA differ from those obtained with a harmonic filter in that its amplitude varies in time, and thus SSA is a useful method for an analysis of quasi-oscillation waves (Vautard et al. 1992). To check this possibility, SSA is applied to the observed and model GMTA after removing their trends. In fact, the 10-yr, about 20-yr, and 5-yr timescale oscillations are identified as leading eigenmodes from the SSA of both observed and model GMTA (not shown). It is also noted that the SSA of observed GMTA produces the 10-yr oscillation as a leading eigenmode among the three timescales, but the leading eigenmode appears at the timescale of about 20 years in the model GMTA.

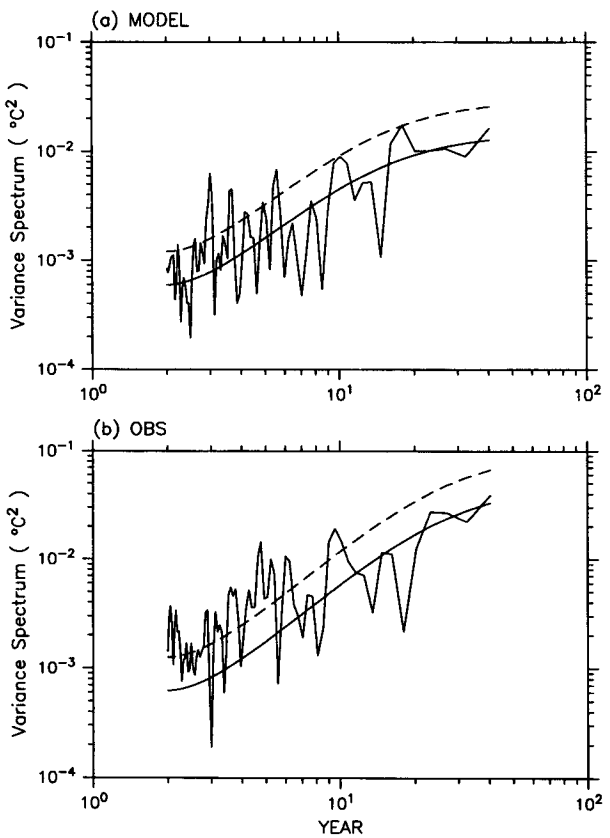

FIG. 4. Power spectrum of global mean surface air temperature anomaly for (a) the model and (b) observation. The solid and dashed lines indicate the level of red noise and the level of 90% confidence for spectral peaks assuming a red noise null hypothesis, respectively.

4. Spatial pattern of surface air temperature fluctuations over the globe

In this section, we identify the global spatial pattern of surface air temperature anomaly associated with GMTA and relate the spatial pattern to a leading eigenmode of the temperature fluctuations over the globe. Figure 5a shows the first eigenvector of surface air temperature simulated by the model. The eigenvector is obtained from the empirical orthogonal function (EOF) analysis of correlation matrix. The first eigenvector explains 8.5% of the total variance over the globe. The figure shows that the eigenvector components have relatively large values over the Tropics, particularly in the Pacific. The time series associated with the eigenvector (Fig. 5b) is characterized by interannual variations on top of interdecadal variations of large amplitude. Note that the time series is similar to that of GMTA shown in Fig. 3a. The correlation coefficient between the two time series is 0.85, which much exceeds a 99% significance level,[1] indicating that the global-mean temperature fluctuations are closely related to the first principal mode of temperature fluctuations over the globe.

The close relationship can be further demonstrated by the global map of correlation coefficient between GMTA and the surface air temperature over the globe. In fact, the correlation map shown in Fig. 6 is very similar to the first eigenvector. Relatively large correlation coefficient appears over the tropical regions, particularly in the Pacific. In contrast to the present results, Stouffer et al. (1994) showed that the large temperature

[1] In the present study, the degree of freedom of correlation coefficient is estimated using the Monte Carlo techniques of Livezey and Chen (1983).

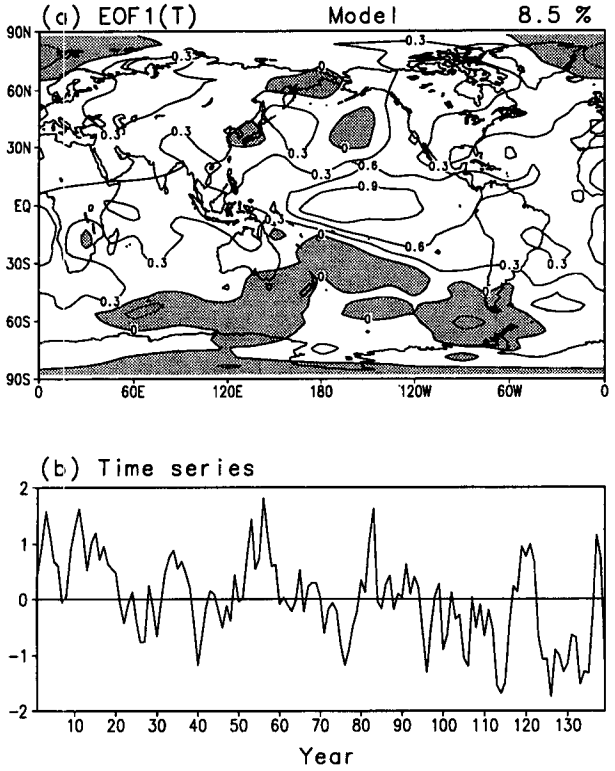

FIG. 5. (a) Distribution of the first eigenvector of surface air temperature over the globe obtained from the EOF analysis. (b) The time series associated with the first eigenvector. Negative values are shaded.

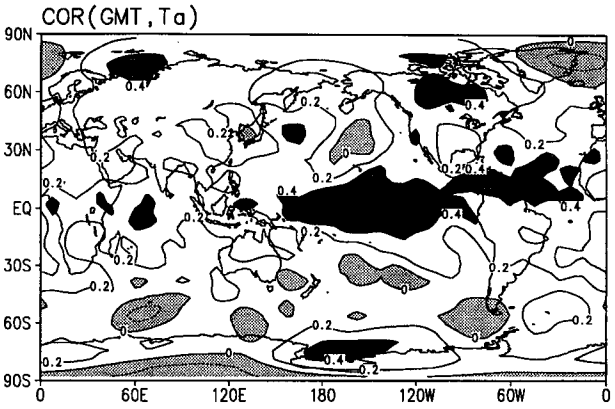

FIG. 6. Distribution of the correlation coefficient between the global mean temperature anomaly (GMTA) and surface air temperature anomaly at each grid point over the globe. Dark shading indicates values larger than 0.4 and negative values are shaded.

anomalies associated with GMTA are located over northern Asia and North America. They used a 1000-yr dataset produced by the same coupled model as used in the present study. Figure 4c of Stouffer et al. shows that the contribution of continental anomalies to GMTA is more than three times larger than the contribution of tropical anomalies. However, the present study shows that the tropical Pacific SST anomalies are more closely related to the GMTA than the continental anomalies. Such difference is not due to different length of data used by the two studies but due to the fact that the anomaly shown by Stouffer et al. can be represented by the correlation coefficient multiplied by the rms of local variation. Actually, the rms values of surface air temperature over the continental regions are about three to four times larger than those of the tropical Pacific region (Fig. 4a in Stouffer et al.). Therefore, the large anomalies associated with GMTA appear over the continental regions, but the anomalies over the tropical Pacific are better correlated with GMTA. It is also interesting to compare Fig. 6 with the corresponding figure (Fig. 12) in Weber and Madden (1995), a somewhat parallel study of a NCAR model. In their figure, large correlations appear over Canada similar to one of the maximum areas in Fig. 6 here, but their results have very little correlation between the equatorial Pacific and the GMTA. This lack of correspondence over the Pacific is undoubtedly related to the fact that the current model data comes from a coupled model, while that of Weber and Madden did not.

The above model results are now compared with the corresponding results obtained with observed data. For this comparison, the observed temperature time series

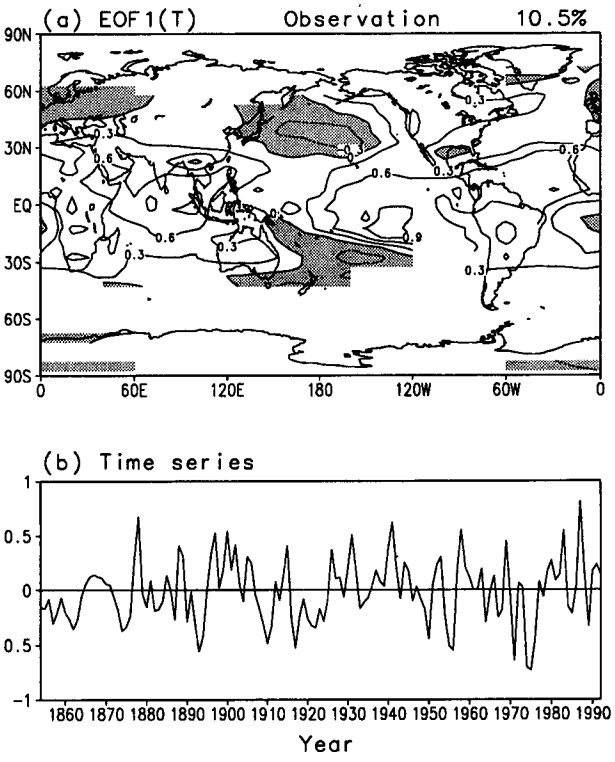

FIG. 7. As in Fig. 5 except for the observation.

is detrended, since the model has only natural variability. The warming trend, which is removed from the observed data at each gridpoint, is made by fitting the second order polynomial to the observed time series for 139 years to consider a relatively small trend in the early period. Figures 7a and 7b present the first EOF eigenvector of the detrended temperature over the globe and its associated time series, respectively. Thus, Figs. 7a and 7b are the observed counterparts of Figs. 5a and 5b, respectively, and they are also based on a correlation matrix. In computing a correlation coefficient between two grid points, all missing data periods appearing in any of the two grid points are eliminated in the computation. It is also noted that the grid points where the period of data available does not exceed 30 years are eliminated in the EOF analysis. Those grids are distributed in the Southern Hemisphere south of 45°S and the Arctic region. Comparison between the observed and model eigenvectors indicates that main features of the model results discussed previously agree reasonably well with those of the observed, although there are differences in some details. In particular, the negative components of the eigenvector in the mid-Pacific are more well organized and the positive center in the tropical Pacific is shifted to the southeast in the observation results. However, it can be said that the model reproduces remarkably well the leading eigenvector of observed temperature fluctuations over the globe. The time series associated with the first eigenvector (Fig. 7b) is characterized by the fluctuations of interannual and interdecadal timescales. Power spectrum analysis indicates that the timescales of distinctive oscillations appear at 3–6 years and about 20 years (not shown). It is noted that the correlation coefficient between the time series of the first eigenvector and observed GMTA is 0.67, which exceeds a 99% significance level.

The above model and observed results show that GMTA is accompanied by the first eigenvector of global temperature that fluctuates with the interannual and interdecadal timescales. To examine the two timescales more clearly, the correlation coefficients between GMTA and the EOF time series are obtained separately for the interannual and interdecadal timescales. For this purpose, a low-pass filter (longer than 7-yr timescale) is applied to GMTA and the EOF1 time series to isolate interdecadal variations. The time filter used is a 31-point digital filter similar to the one used by Knutson and Weikmann (1987) and Kang and Lau (1990). The interdecadal time series thus obtained is subtracted from the original time series to obtain the interannual time series that has the timescales less than 7 years. The use of 7-yr timescale for the separation is due to the fact that the interdecadal and interannual timescales are well separated by 7–8-yr timescales (Figs. 4a and 4b). All correlation coefficients, shown in Table 2, are statistically significant, confirming that the global-mean temperature fluctuations of both timescales in the model and observation are closely related to the first eigenvector. Again, it is noted that the first eigenvectors of the model and observation have large components over the tropical Pacific, indicating that the tropical Pacific plays an important role in global-mean temperature fluctuations. In the next section, we examine the variability of tropical Pacific SST in more detail and relate the variability to global-mean temperature fluctuations.

TABLE 2. Correlation coefficients between the GMTA and EOF1(T) time series for interannual and interdecadal timescales.

	Interannual timescales	Interdecadal timescales
Model	0.68	0.91
Observation	0.63	0.72

5. Principal modes of tropical Pacific SST fluctuations

The principal modes of tropical Pacific SST fluctuations of the model are obtained and compared with those obtained with the observed SST for the 42-yr period of 1950–1992. Since the tropical Pacific SST fluctuations are focused on here, the analysis domain is confined to the tropical Pacific between 30°S and 30°N. Again annual means are used in this section. To compare the model results with observed counterparts, it may be necessary to eliminate trends in the observed SSTs. Therefore, as with the observed air temperature, a second-order polynomial trend is removed from the observed SST time series at each grid point in the domain.

The EOF modes of model SST are shown in Fig. 8. The first eigenvector displayed in Fig. 8a explains 23.6% of total variance. Its spatial pattern is characterized by a same sign in most of the domain, except in the southern subtropics, and is reminiscent of the SST anomalies during a mature phase of the El Niño (Rasmusson and Carpenter 1982). The time series associated with the first eigenvector shown in Fig. 8b is characterized by interannual fluctuations on top of interdecadal oscillations of relatively large amplitude. Power spectrum analysis (not shown) indicates that two pronounced spectral peaks appear at about 20 and 9 years and relatively small peaks at 4–5-yr timescales. These spectral characteristics are similar to those of GMTA shown in Fig. 4a. The connection between the EOF1 and GMTA is further demonstrated by the correlation coefficient 0.58 between the two time series that is above a 99% significance level. It is also noted that the correlation coefficient between the time series shown in Figs. 8b and 5b is 0.86, indicating that the EOF1 of global temperature is closely related to the EOF1 of tropical Pacific SST.

The second eigenvector, which explains 6.1% of total variance, is shown in Fig. 8c. In the figure, positive

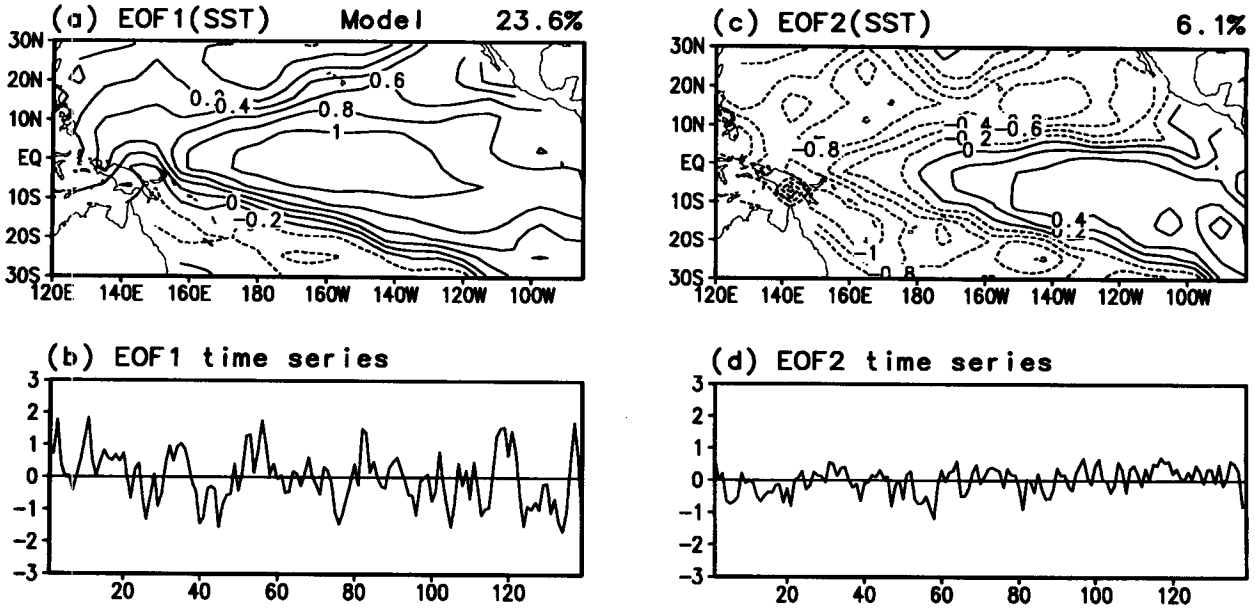

FIG. 8. Principal modes of annual-mean SST fluctuations of the coupled model over the tropical Pacific obtained by using the EOF analysis. (a), (b) The first eigenvector and the associated time series, respectively. (c), (d) The second mode. Units are arbitrary.

components are distributed over the region extending from the eastern Pacific to the central equatorial Pacific and negative components over the western equatorial Pacific and the subtropical Pacific Oceans in both hemispheres. The spatial pattern looks similar to an observed SST anomaly pattern during one phase of the El Niño. In contrast to the first eigenvector, the time series of the second eigenvector (Fig. 8d) does not show interdecadal variations, but it is dominated by timescale variations of a few years. Lau et al. (1992) analyzed an ENSO-like phenomena using a long-term simulation of a coupled model similar to the one used in this study but without a seasonal cycle. Their results of the extended EOF analysis showed that SST anomalies make their first appearance off the Peru–Ecuador coast and then migrate steadily westward with an average transit time of 12–15 months. Comparisons of the present eigenvectors with the extended EOF results of Lau et al. indicate that the first and second eigenvectors, shown in Figs. 8a and 8c, respectively, seem to describe different phases of the ENSO-like phenomena in the interannual timescale. The interdecadal oscillation, on the other hand, is described only by the first eigenvector.

The principal modes of the model SST are compared with those of the observed SST. The first and second eigenvectors of the observed SST shown in Figs. 9a and 9c explain 39.1% and 14.1% of total variance, respectively. Comparisons show that the spatial patterns of the observed eigenvectors are very similar to the model counterparts, except that the percentage variance of the observed eigenvectors are bigger than that of the model. The difference of the percentage variance can result from the use of different data lengths. However, it is more likely that the smaller percentage variance of the model may be due to the fact that the model variance of the tropical Pacific SST is much less than that of the observed, particularly in the interannual ENSO timescales (Lau et al. 1992; Knutson and Manabe 1995). The time coefficient associated with the first eigenvector is shown in Fig. 9b. It has a large positive value at most of El Niño years. In contrast to the pronounced interdecadal oscillations of the model principal mode, it is hard to identify interdecadal oscillations in Fig. 9b mainly due to the relatively short data length. Nitta and Yamada (1989) showed that the characteristics of the observed Pacific SST after mid-1970 are different from that before 1970. But such a feature is not clear in Fig. 9b because the trend is eliminated in the present study.

6. Summary and concluding remarks

Long-term variability of global-mean surface air temperature and the related principal modes of surface air temperature over the globe and those of tropical Pacific SST are investigated by using data from a coupled ocean–atmosphere model 139-year simulation and the observed datasets of surface air temperature over the globe for 139 years and tropical Pacific SST for 42 years. Both global-mean surface air temperatures of the model and observation are characterized by interdecadal oscillations with timescales of about 20 and 10 years and interannual fluctuations with timescales

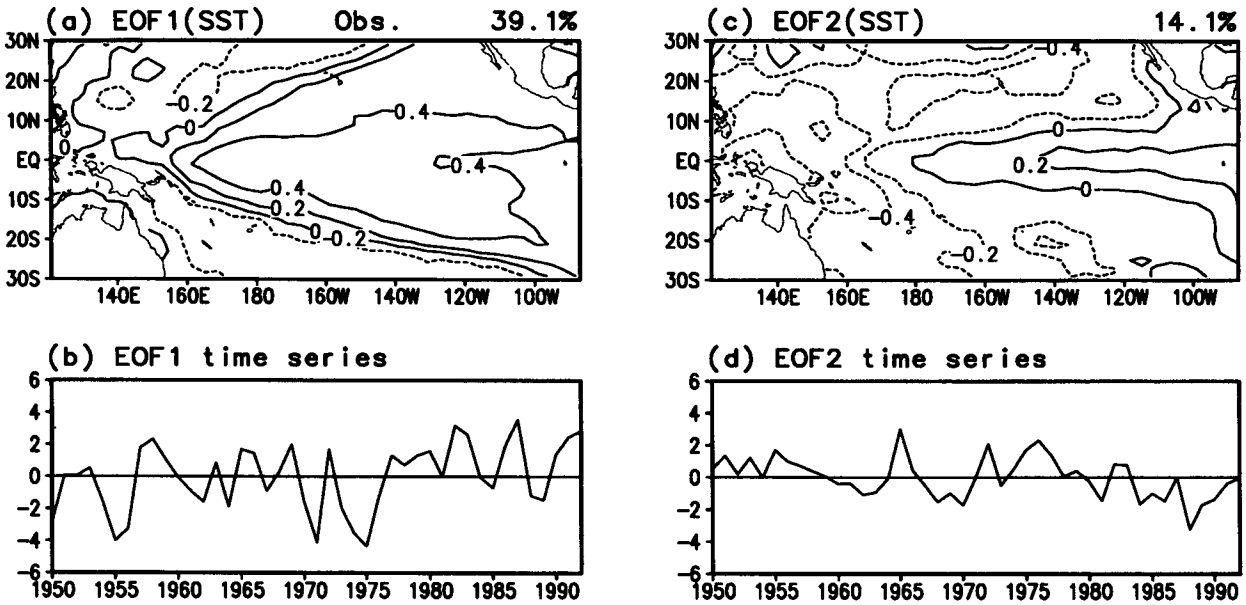

FIG. 9. As in Fig. 8 except for the observed SST.

of 3–6 years. As in previous studies, the interannual fluctuations are associated with the ENSO-like phenomena. Also demonstrated in the present study is that the interdecadal oscillations are also related to the variations of tropical Pacific SST whose spatial pattern similar to the ENSO. In fact, both interdecadal and interannual variations of global-mean temperature are related to the first principal mode of tropical Pacific SST.

It should be mentioned that the present model produces relatively weak interannual variability of global-mean temperature compared with observation. The weak interannual variability is related to the weak SST anomalies during the El Niño in the model. As indicated by Lau et al. (1992), the low-resolution coupled model used in the present study simulates ENSO-like phenomena with relatively small amplitude. But, the companion paper by Philander et al. (1992) showed that their high-resolution coupled model is able to simulate the ENSO more realistically. By comparing their results with those of Philander et al., Lau et al. discussed that the nature of the model ENSO depends very much on the resolution of ocean model. In the present study, however, we do not focus on the model ability of the ENSO simulation but link the fluctuations of GMTA to tropical SST fluctuations. Moreover, it is pointed out that the ENSO has interdecadal variations that seem to be a more distinctive feature than the interannual variations in the model.

The timescales of interannual and interdecadal oscillations are well separated from each other. Thus, it may be interesting to investigate the interdecadal oscillation by separating those timescales from the long-term data of the model and observation. In particular, the time evolution of circulation statistics and the associated dynamics should be studied to demonstrate more clearly the existence of interdecadal oscillations forced by the tropical Pacific. There have been several studies of interdecadal variations of the Pacific SST (Nitta and Yamada 1989; Wang 1995), which suggested the existence of interdecadal variations of the ENSO. But the data length of about 40 years that they used may not be sufficient to extract common features of interdecadal variability. Because of a lack of sufficient historical data, a good approach would be to use the ocean–atmosphere coupled model for such studies. These topics are deserving of future research.

The sampling error of the observed GMTA arising from missing data points, which are different in time for 139 years of 1854–1992, is also examined by using the model data. The present study indicates that the sampling error of natural variability of GMTA is not small even for recent years. In recent 59 years after 1934, the mean error and rms error of sampled annual-mean GMTA for each 20-yr segment are about 0.01°C and 0.03°C, respectively, indicating that for recent decades the sampling error of the observed GMTA seldom (less than 2.5%) exceeds 0.07°C. Although there are some differences between the global mean and the sampled global mean as indicated above, the correlation coefficient between the two time series for 139-yr period is 0.93, indicating that long-term variations of the global mean is reasonably well represented by the sampled global mean.

Acknowledgments. The author wants to express his sincere appreciation to Drs. S. Manabe and T. Knutson

at GFDL for providing a GFDL coupled model data and encouraging the author to continue the present study. He also appreciates T. Smith at NMC for providing SST data. H.-K. Kim, S.-I. An, and K.-M. Kim at Seoul National University are also thanked for their contribution to this study. This research was supported by G7 project, the Ministry of Environment, and the Basic Science Research Institute Program, the Ministry of Education, Korea.

REFERENCES

Bjerknes, J., 1966: A possible response of the atmospheric Hadley circulation to equatorial anomalies of ocean temperature. *Tellus,* **18,** 820–829.

Bryan, K., 1969: Climate and the ocean circulation. Part III: The ocean model. *Mon. Wea. Rev.,* **97,** 806–827.

——, and L. J. Lewis, 1979: A water mass model of the World Ocean. *J. Geophys. Res.,* **84(C5),** 2503–2517.

Elsner, J. B., and A. A. Tsonis, 1991: Do bidecadal oscillations exist in the global temperature record. *Nature,* **353,** 551–553.

Folland, C. K., D. E. Parker, and F. E. Kates, 1984: Worldwide marine temperature fluctuations 1856–1981. *Nature,* **310,** 670–673.

Ghil, M., and R. Vautard, 1991: Interdecadal oscillations and the warming trend in global temperature time series. *Nature,* **350,** 324–327.

Hansen, J., and S. Lebedeff, 1987: Global trends of measured surface air temperature. *J. Geophys. Res.,* **92,** 13 345–13 372.

Horel, J. D., and J. M. Wallace, 1981: Planetary-scale atmospheric phenomena associated with the Southern Oscillation. *Mon. Wea. Rev.,* **109,** 813–829.

Jacobs, G. A., H. E. Hurlburt, J. C. Kindle, E. J. Metzger, J. L. Mitchell, W. J. Teague, and A. J. Wallcraft, 1994: Decade-scale trans-Pacific propagation and warming effects of an El Niño anomaly. *Nature,* **370,** 360–363.

Jones, P. D., S. C. B. Raper, R. S. Bradley, H. F. Diaz, P. M. Kelly, and T. M. L. Wigley, 1986: Northern Hemisphere surface air temperature variations: 1851–1984. *J. Climate Appl. Meteor.,* **25,** 161–179.

Kang, I.-S., and K.-M. Lau, 1990: Evolution of tropical circulation anomalies associated with 30–60 day oscillation of globally averaged angular momentum during Northern summer. *J. Meteor. Soc. Japan,* **68,** 237–249.

Keppenne, C. L., and M. Ghil, 1991: Adaptive spectral analysis and prediction of the Southern Oscillation index. *Proc. 15th Climate Diagnostics Workshop,* NMC/NOAA, 30–35.

Knutson, T. R., and K. M. Weikmann, 1987: 30–60 day atmospheric oscillation: Composite life cycles of convection and circulation anomalies. *Mon. Wea. Rev.,* **115,** 1407–1436.

Lau, N.-C., S. G. H. Philander, and M. J. Nath, 1992: Simulation of ENSO-like phenomena with a low-resolution coupled GCM of the global ocean and atmosphere. *J. Climate,* **5,** 284–307.

Livezey, R. E., and W. Y. Chen, 1983: Statistical field significance and its determination by Monte Carlo techniques. *Mon. Wea. Rev.,* **111,** 46–59.

Madden, R. A., and G. E. Meehl, 1993: Bias in the global mean temperature estimated from sampling a greenhouse warming pattern with the current surface observing network. *J. Climate,* **6,** 2486–2489.

——, D. J. Shea, G. W. Branstator, J. J. Tribbia, and R. O. Weber, 1993: The effects of imperfect spatial and temporal sampling on estimates of the global mean temperature: Experiments with model data. *J. Climate,* **6,** 1057–1066.

Manabe, S., K. Bryan, and M. J. Spelman, 1990: Transient response of a global ocean–atmosphere model to a doubling of atmospheric carbon dioxide. *J. Phys. Oceanogr.,* **20,** 722–749.

——, R. J. Stouffer, M. J. Spelman, and K. Bryan, 1991: Transient responses of a coupled ocean–atmosphere model to gradual changes of atmospheric CO_2. Part I: Annual mean response. *J. Climate,* **4,** 785–818.

Namias, J., X. Yuan, and D. R. Cayan, 1988: Persistence of North Pacific sea surface temperature and atmospheric flow patterns. *J. Climate,* **1,** 682–703.

Newell, N. E., R. E. Newell, J. Hsiung, and Z. Wu, 1989: Global marine temperature variation and the solar magnetic cycle. *Geophys. Res. Lett.,* **16,** 311–314.

Nitta, T., and S. Yamada, 1989: Recent warming of tropical sea surface temperature and its relationship to the Northern Hemisphere circulation. *J. Meteor. Soc. Japan,* **67,** 375–383.

Philander, S. G. H., R. C. Pacanowski, and N.-C. Lau, 1992: Simulation of ENSO with a global atmospheric GCM coupled to a high-resolution tropical Pacific Ocean GCM. *J. Climate,* **5,** 308–329.

Rasmusson, E. M., and T. H. Carpenter, 1982: Variations in tropical sea surface temperature and surface wind fields associated with the Southern Oscillation/El Niño. *Mon. Wea. Rev.,* **110,** 354–384.

Stouffer, R. J., S. Manabe, and K. Ya. Vinnikov, 1994: Model assessment of the role of natural variability in recent global warming. *Nature,* **367,** 634–636.

Vautard, R., P. Yiou, and M. Ghil, 1992: Singular spectrum analysis: A toolkit for short, noisy chaotic signals. *Physica D.,* **58,** 95–126.

Wang, B., 1995: Interdecadal changes in El Niño onset in the last four decades. *J. Climate,* **8,** 267–285.

Weber, R. O., and R. A. Madden, 1995: Optimal averaging for the determination of global mean temperature: Experiments with model data. *J. Climate,* **8,** 418–430.